5-28-2017

Reduced-mobility layers with high internal mobility in poly(ethylene oxide)-silica nanocomposites

Yury Golitsyn
Martin-Universität Halle-Wittenberg

Gerald J. Schneider
Louisiana State University

Kay Saalwächter
Martin-Universität Halle-Wittenberg

Recommended Citation

Golitsyn, Y., Schneider, G., & Saalwächter, K. (2017). Reduced-mobility layers with high internal mobility in poly(ethylene oxide)-silica nanocomposites. *Journal of Chemical Physics, 146* (20) https://doi.org/10.1063/1.4974768

The Journal of Chemical Physics

Reduced-mobility layers with high internal mobility in poly(ethylene oxide)–silica nanocomposites

Cite as: J. Chem. Phys. **146**, 203303 (2017); https://doi.org/10.1063/1.4974768
Submitted: 07 November 2016 • Accepted: 29 December 2016 • Published Online: 02 February 2017

Yury Golitsyn, Gerald J. Schneider and Kay Saalwächter

AIP Publishing

Reduced-mobility layers with high internal mobility in poly(ethylene oxide)–silica nanocomposites

Yury Golitsyn,[1] Gerald J. Schneider,[2] and Kay Saalwächter[1,a)]
[1]*Institut für Physik–NMR, Martin-Luther-Universität Halle-Wittenberg, Betty-Heimann-Street 7, D-06120 Halle, Germany*
[2]*Department of Chemistry and Department of Physics, Louisiana State University, Baton Rouge, Louisiana 70803, USA*

(Received 7 November 2016; accepted 29 December 2016; published online 2 February 2017)

A series of poly(ethylene oxide) nanocomposites with spherical silica was studied by proton NMR spectroscopy, identifying and characterizing reduced-mobility components arising from either room-temperature lateral adsorption or possibly end-group mediated high-temperature bonding to the silica surface. The study complements earlier neutron-scattering results for some of the samples. The estimated thickness of a layer characterized by significant internal mobility resembling backbone rotation ranges from 2 nm for longer (20 k) chains adsorbed on 42 nm diameter particles to 0.5 nm and below for shorter (2 k) chains on 13 nm particles. In the latter case, even lower adsorbed amounts are found when hydroxy endgroups are replaced by methyl endgroups. Both heating and water addition do not lead to significant changes of the observables, in contrast to other systems such as acrylate polymers adsorbed to silica, where temperature- and solvent-induced softening associated with a glass transition temperature gradient was evidenced. We highlight the actual agreement and complementarity of NMR and neutron scattering results, with the earlier ambiguities mainly arising from different sensitivities to the component fractions and the details of their mobility. [http://dx.doi.org/10.1063/1.4974768]

I. INTRODUCTION

Particle-filled polymers, in particular elastomers for, e.g., tire applications, display outstanding mechanical properties as compared to the pure material.[1] The unique reinforcement has been explained theoretically[2,3] as well as experimentally[4–6] by filler networking, where filler-filler contacts are mediated by adsorbed and thus immobilized polymer species. The characterization of such adsorbed layers is challenging, as the traditional solvent-leaching technique ("bound rubber determination") largely overestimates the amount of polymer being part of the actual reduced-mobility layer.[7]

Surface-adsorbed and thus immobilized species are thus of high scientific interest. They are specific for polymers displaying attractive interactions with either the bare or the surface-modified filler. Bare oxide fillers such as silica and alumina, displaying surface hydroxy groups, interact favorably with polymers capable of acting as hydrogen-bond acceptor, such as poly(dimethyl siloxane), PDMS,[8–10] poly(ethylene oxide), PEO,[11–15] poly(2-vinyl pyridine), P2VP,[16,17] or different acrylate polymers.[5,18–22]

The amount of dynamically modified polymer, and with this the nominal thickness of an assumed-to-be contiguous reduced-mobility layer, can be estimated on the basis of results from different techniques. Such results are often not compatible with each other even for virtually the same polymer-surface system and the same method.[12–14] In this context DSC,[10,16,19] dielectric spectroscopy,[23,24] NMR spectroscopy,[13,18,20,21] and static[22] as well as dynamic[9,11,12,14,15] neutron scattering techniques have been used. Apart from purely structural (=density) information obtained by static scattering,[22] most other techniques are sensitive to dynamic properties. Also DSC, mostly probing changes in the glass transition temperature (T_g), is related to a slowdown of segmental relaxation and thus dynamics.

Since the different methods probe molecular dynamics or derived quantities in different ways, a certain level of disagreement between the different results should not be surprising. For example, the notion of a "glassy layer" has emerged[1,4,13,18,20] but is subject to ambiguity as this implies literally that the reduced-mobility components are below their T_g, i.e., have a cooperative segmental relaxation time (τ_α) of at least 100 s at the temperature of measurement, and may exhibit only rather localized faster motions (β and higher relaxations). Therefore, conclusions based upon neutron-scattering observations at comparably high temperatures, stating the absence of a "glassy" layer[9] or even claiming "contradiction"[14] to earlier NMR results,[13] originate partially from the simplistic nomenclature and, specifically, a lack of a more detailed discussion of the layer properties in Ref. 13.

To highlight the range of phenomena, e.g., PDMS adsorbed on silica in a porous system exhibits a separate T_g as directly observed by DSC,[10] while an acrylate polymer adsorbed on silica spheres was proven to feature a gradient in T_g.[21] In the latter case, DSC observations of a broadening

a)Electronic address: kay.saalwaechter@physik.uni-halle.de. URL: www.physik.uni-halle.de/nmr

of the T_g-related step could be quantitatively reproduced by a model based upon a τ_α profile derived from quantitative NMR data, the latter being sensitive to τ_α once it is less than 0.1 ms.[20] In extending this picture, Napolitano has further advocated the discussion of a lowermost "dead layer,"[23] which remains immobilized and does not devitrify[19] at all accessible temperatures.

Here, we present an NMR study of different nanocomposites composed of PEO with different endgroups in interaction with silica nanospheres. We compare samples previously studied by neutron spin-echo (NSE) and time-of-flight (TOF) spectroscopy[14,15] with a sample from a series previously studied by NMR[13] and highlight the qualitative differences. We can thus reconcile previous conclusions on a potential disagreement of neutron-scattering and NMR results—which turn out to be only apparent. We address the indeed substantial internal mobility of the adsorption layer,[9] and assess changes arising from changes in temperature, annealing times, and water content. Different influencing factors, such as the molecular weight, endgroups, and confinement geometry (spheres of different diameters vs. pores), are discussed.

II. EXPERIMENTAL

A. Samples

We compare 3 nanocomposite samples made of a short-chain PEO (molecular weight about 2 kg/mol) with variable endgroups mixed with silica spheres of $d = 12.8$ nm diameter at a filler volume fraction $\phi_f = 0.15$. The samples were prepared by solution blending as described in Refs. 14 and 15 and consist of mixtures of protonated and perdeuterated chains, as they were prepared for neutron scattering studies. With ^{1}H NMR we of course only detect the protonated chains. These samples feature an internal silica surface-to-volume ratio (S/V) of about 0.07 nm^{-1} and a mean filler-filler surface distance of about 15 nm as simplistically estimated from an assumed cubic arrangement. Another sample made from OH-terminated PEO of 20 kg/mol mixed with silica spheres of about 42 nm diameter at $\phi_f = 0.4$ was prepared by a very similar procedure as described in Ref. 13. For the latter, despite the higher ϕ_f the S/V of the sample is only about 20% lower and the mean filler-filler distance is about 40% higher, which means that all samples are comparable in these regards. The samples were sealed in glass tubes that had been evacuated for 2 h at ambient temperature and studied at temperatures between 70 °C and 140 °C, i.e., above the melting temperature of PEO. The sample characteristics are summarized in Table I.

In order to study the effect of water contents, the sample tube of PEO20k-42-OO was opened and stored in a desiccator containing a water reservoir (RH = 100%) for 17 h and then re-sealed for measurements at a variable temperature (PEO20k-42-humid). Afterwards, the sample was again opened, dried in vacuum for 22 h at 50 °C, re-sealed, and again measured (PEO20k-42-dried). The actual water uptake and its effect on the results are discussed below.

B. ^{1}H NMR

^{1}H NMR experiments were performed on a 200 MHz Bruker Avance III spectrometer using a static 5 mm Bruker probe with a short dead time (2.5 μs). Temperature regulation was based upon a stream of heated or cooled air, with an accuracy of about ±1 K and a ~0.5 K temperature gradient over the sample. 90° pulses of 2 μs length and recycle delays (d_1) of at least $5T_1$ (estimated at each given temperature) were applied. Free-induction decay (FID) signals were acquired exactly on-resonance in pure-absorption mode, analyzing only the decaying real part of the signal (the imaginary part is always near zero). To overcome the dead time before detection, we used the mixed magic-sandwich echo, MSE.[25,26] Furthermore, the magic and polarization echo, MAPE,[27] and 2-pulse-segment double-quantum (DQ) sequences were used as filters to selectively detect the most mobile and most immobile sample fractions, respectively.[28,29] All FIDs were only analyzed up to $t = 200$ μs acquisition time, since at longer acquisition times field-inhomogeneity and sample susceptibility effects distort the signal and preclude proper fitting.[28,29]

TABLE I. Sample characteristics.

Sample[a]	End groups	Silica volume fraction	Immobilized fraction[b] (%)	Layer thickness[b] (nm)
PEO2k-13-OO	2 × OH	0.15	3.72	0.49
PEO2k-13-CC	2 × CH_3	0.15	0.88	0.12
PEO2k-13-OC	OH/CH_3	0.15	1.87	0.26
PEO20k-42-OO	2 × OH	0.4	13.1	2.08

[a]The sample name encodes the PEO molecular weight (g/mol) and the silica diameter (nm).
[b]Measured at 70 °C.

III. RESULTS AND DISCUSSION

A. Dynamic component decomposition

^{1}H NMR results for all samples are compared in Fig. 1. The amplitude of the normalized FID detected after an excitation pulse represents the integral signal of all protons in the system, subject to relaxation, more specifically, dephasing by multiple dipole-dipole couplings. These couplings are orientation dependent, such that the observed relaxation behavior, i.e., the shape of the decaying FID, informs about the respective amount of protons in chemical moieties subject to—potentially localized—rotational motion on a characteristic time scale and with characteristic amplitude.

For polymer components with reduced or even absent mobility (no large-angle segmental jumps), the FID shape is close to a Gaussian, $\exp\left[-(t/T_{2,\mathrm{stat}})^2\right]$. In case of polymers with CH_2 groups, featuring a dominant coupling between the two protons, the decay time constant $T_{2,\mathrm{stat}}$ (at which the signal has decayed by about ~65%) is of the order of 12–15 μs.[29] This characteristic $T_{2,\mathrm{stat}}$ is about twice the inverse average dipole-dipole coupling constant D_{HH} (unit: rad/s), i.e., $D_{\mathrm{HH}}^{-1} \approx (2\pi \times 20\ \mathrm{kHz})^{-1} \approx 8$ μs. Large-angle jumps with correlation times on this time scale ($\tau_c \approx T_{2,\mathrm{stat}}$) lead to significant changes of the shape of the FID. For example, if the jump process is nearly isotropic (as is the case for the α relaxation associated with the glass transition), heating (i.e., decreasing $\tau_c = \tau_\alpha$) affords a progressive reduction of the coupling strength and a smooth transition to a more exponential decay

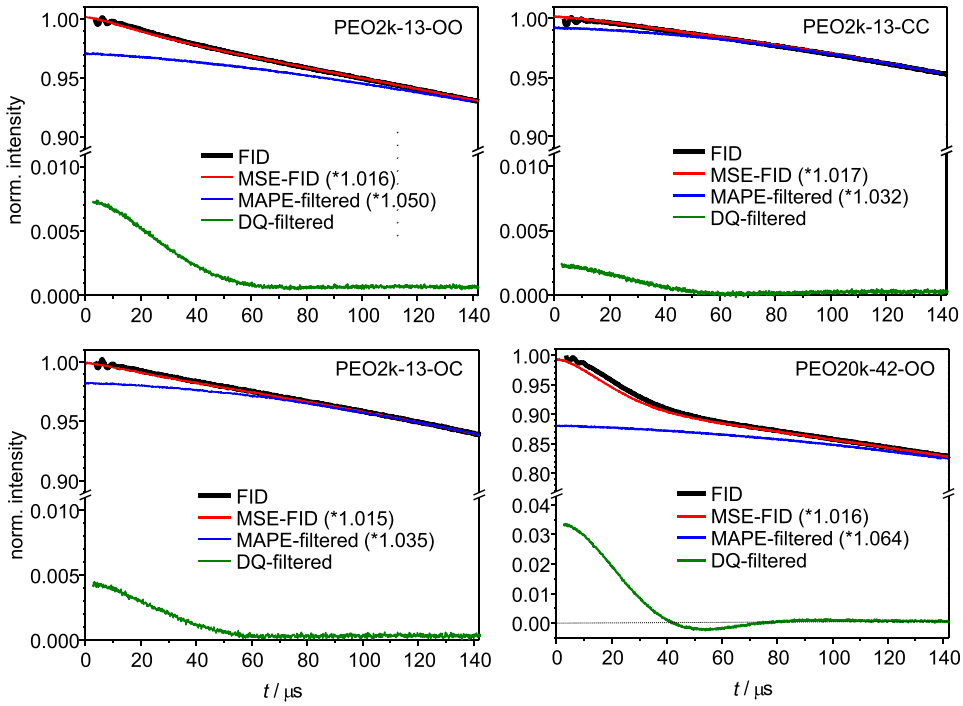

FIG. 1. Comparison of ^{1}H NMR data used for dynamic component decomposition in the 4 investigated samples at 70 °C. All data except for PEO20k-42-OO with its higher immobilized-phase contents are plotted on the same vertical scales. The MSE-refocused and MAPE-filtered data are nearly quantitative for the total and mobile-component signal, respectively, as demonstrated by the small indicated intensity corrections (MAPE-filtered data were scaled to match the FID intensity at $t = 200\,\mu$s).

with a decay time constant (T_2^*) reaching at least the millisecond range.[20] Note that NMR probes the α relaxation in the high frequency range far above T_g, due to the specific value of $T_{2,\mathrm{stat}}$.

This phenomenology provides the basic distinction between segments that reorient comparably slowly and/or with low angular amplitude ("rigid") or rapidly with larger angular amplitude ("mobile"). As is apparent from the data in Fig. 1, the sample signals are largely dominated by components with comparably long T_2^* as expected from a substance far above its T_g. However, the FIDs also feature sub-components in the % range that appear more "rigid." Segments in such a component (subject to an increase in T_g by confinement or adsorption effects) do not move significantly in lateral direction and are usually considered to be part of a contiguous sub-volume that is reasonably assumed to form a layer around the filler particles.[20]

In such a dynamically inhomogeneous system, the FID can be written as a superposition, where typically no more than 3 distinct components, including an intermediate one, can be differentiated according to[28,29]

$$\frac{\mathrm{FID}(t)}{\mathrm{FID}(t=0)} = a_r \exp\left[-M_2 t^2/2\right] + a_i \exp\left[-(t/T_{2,\mathrm{i}}^*)^{\beta_i}\right] + (1-a_r-a_i)\exp\left[-(t/T_{2,\mathrm{m}}^*)^{\beta_m}\right]. \quad (1)$$

The decay of the most immobilized species is usually described by a Gaussian with M_2 being the second moment of the dipolar frequency distribution ($M_2 = 2T_{2,\mathrm{r}}^{*\,-2} \approx \frac{9}{20}D_{\mathrm{HH}}^2$), which also subsumes the action of multiple remote couplings. In the rigid limit, this value depends on the average distances between the protons, i.e., their density. Here, were refer to this component as "rigid," but note that rather fast ($\tau_c \ll 10\ \mu$s) but strongly anisotropic, i.e., geometrically constrained motion, also leads to a Gaussian decay but with an M_2 lower than predicted from the proton density (due to, e.g., a β process). As mentioned above, more isotropic larger-amplitude motions on the time scale of the inverse effective coupling lead to a qualitative change in the decay shape, usually well described by a compressed (exponent $\beta > 1$) or stretched ($\beta < 1$) exponential function with a characteristic decay time T_2^*. This *ansatz* is thus chosen for the other two components. It is stressed that in the realistic case of a mobility gradient,[21] the fitting function merely represents a minimal-parameter model.

Fits to Eq. (1) are not necessarily stable, so additional experiments are recommended. First, the significant receiver dead time and ambiguities due to potential short-time oscillations arising from probe ring-down should be overcome. This can be achieved by the MSE, which in Fig. 1 is seen to provide near-quantitative refocusing. Despite the only small loss of less than 2%, the full fit is always performed for the bare FID. The MSE is, however, used for detection in the filtering experiments.

The DQ and MAPE filters select the "rigid" and mobile components, respectively, and the filtering times do have some influence on the actual component attribution, see Ref. 29 for details on their choice. While the DQ-filtered signal is non-quantitative due to the impossibility to transiently convert all related signal into DQ coherences, the MAPE-filtered signal is ideally identical to the FID at longer times at which the less mobile components have decayed. This is demonstrated to be the case in Fig. 1. Both *filtered* signals can be fitted to the associated *individual* fit functions, thus determining the respective shape parameters (M_2 or $T_{2,\mathrm{m}}$,β_m, respectively). Note that the DQ-filtered data feature a small oscillation around 50 μs due to residual spin-pair character. While one could use a more complicated fitting function to capture this phenomenon,[29] we here chose to approximate it with a Gaussian, with negligible overall error. It is also stressed that $T_{2,\mathrm{m}}$ and β_m can be determined from the MAPE-filtered signal with high precision despite the limited fitting range.

The pre-determined parameters are then held fixed in the final multi-parameter fit to the FID. This allows for a reliable fit of the remaining shape parameters of the intermediate component ($T_{2,i}$, β_i) and the three signal fractions. The results of the component decomposition for one of the samples are plotted in Fig. 2. The FID shape for slowly relaxing components may be dominated by instrumental imperfections, mainly the magnetic-field inhomogeneity. This is why $T_{2,m}$ and β_m are not necessarily meaningful in quantifying mobility; other experiments (multiple-quantum NMR or neutron scattering) are more suitable to characterize the most mobile, melt-like majority component in detail.[13–15,20] In Table II we therefore summarize the results for the reduced-mobility components, to which we restrict our discussion.

Additional signal contributions may arise from immobilized water and –OH groups associated with the silica surface. This issue was already discussed in our earlier work,[13] to which we refer for details. We here just note that their contribution is estimated to be lower than the given error margin.

The results for sample PEO2k-13-OC may serve as an example of potential ambiguities and limitations related to distinguishing the most immobilized and the "intermediate" fraction, the latter usually being associated with a transition region featuring a mobility gradient. A value of $M_2 \approx 1600$ ms^{-2} was obtained by a fit to the DQ-filtered data, yet the joint fit assigned a fraction of 0 to this most immobilized part. Since $M_2 = 2T_{2,r}^{*\,-2}$, the given value corresponds to a $T_{2,r}^*$ of 35 μs. It is thus realized that the fitted intermediate fraction with a similar $T_{2,i}^*$ but modified exponent of 1.36 was sufficient to describe the whole immobilized fraction. In all, the data in Table II demonstrate that the effective mobility of the intermediate fraction does not deviate much from the "rigid" component, suggesting that the two components should be discussed together. The overall absolute error for the sum of the components is estimated to about 0.2%. Only for sample PEO20k-42-OO are the signal large and the dynamic inhomogeneity substantial enough to reliably distinguish three components. Most notably, the observed range of apparent $T_{2,r}^*$ values of 28–35 μs as calculated from the M_2 values significantly exceeds the $T_{2,stat}$ expected for immobile CH_2 groups, suggesting high internal mobility.

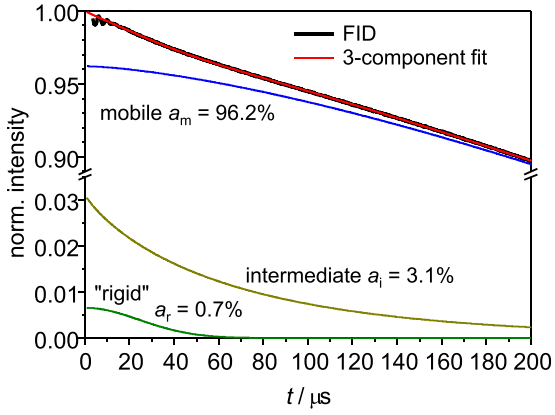

FIG. 2. FID signal for sample PEO2k-13-OO at 70 °C (thick black line) and its fit, along with the fitted signal components (thin lines).

TABLE II. Reduced-mobility fractions determined by ^{1}H NMR signal decomposition and associated decay shape parameters.

Sample	"Rigid"	Intermediate
PEO2k-13-OO	a_r = 0.66% M_2 = 1710 ms^{-2}	a_i = 3.06% T_2^* = 65.3 μs β = 0.85
PEO2k-13-CC	a_r = 0.18% M_2 = 1623 ms^{-2}	a_i = 0.70% T_2^* = 37.0 μs β = 1.53
PEO2k-13-OC	a_r = 0.0% M_2 = 1761 ms^{-2}	a_i = 1.87% T_2^* = 36.62 μs β = 1.36
PEO20k-42-OO	a_r = 6.08% M_2 = 2620 ms^{-2}	a_i = 7.16% T_2^* = 70.5 μs β = 0.74

B. Layer thickness

The fractions listed in Table II demonstrate that all four samples display significantly different reduced-mobility components despite the comparable specific filler surface area. The summed immobilized fraction of PEO20k-42-OO of about 13% corresponds well to the results from our previous study,[13] where it was shown that a fraction of this order in similar samples is independent of molecular weight in a range of 0.3 to 20 kg/mol. This latter finding is important and clearly excludes that the end groups play a significant role in determining the amount and properties of the reduced-mobility components in this specific case.

For a better comparison with the literature data, we assume that the total immobilized fraction is restricted to a contiguous spherical shell (thus neglecting particle contacts) with layer thickness

$$\delta = \frac{d}{2}\left[\left(\frac{a_r + a_i}{\phi_f} + 1\right)^{1/3} - 1\right], \qquad (2)$$

with d the sphere diameter and ϕ_f the filler volume fraction. Note that this formula corrects the somewhat simplified approach of Ref. 13, where a cuboid of height δ with a surface equivalent to that of the sphere was assumed, i.e., curvature was neglected (the error is negligible for the 44 nm particles studied there). Results for $a_r + a_i$ and δ are included in Table I. Again, the summed layer thickness for PEO20k-42-OO is comparable to what was measured by Kim *et al.* for samples of widely variable molecular weight and different silica volume fractions, which ranged between 1.5 and 3 nm.[13]

The PEO2k-13 samples exhibit significantly thinner albeit in all cases clearly detectable immobilized layers. Apart from differences in the temperature treatment (see below), the possibly most relevant difference between these and the PEO20k-42-OO sample is the significantly lower particle diameter. In agreement with this finding, thinner 1 nm layers of P2VP adsorbed to 15 nm silica spheres vs. a 4–5 nm layer on a flat silica surface have recently been found by Kumar and coworkers.[16] Our data comply with this range. The origin of such a curvature dependence, and the relevance of chemical detail, is yet to be elucidated.

The rather thin 0.49...0.12 nm layers found for the PEO2k-13 series exhibit a clear dependence on the endgroups (see Table I), with doubly OH-terminated (OO) chains showing a thicker layer than the doubly methyl-terminated (CC) chains, with the mixed OC case lying in-between. The Å-scale "layer" formed by the CC chains is nominally thinner than the PEO backbone, suggesting less-than-monolayer coverage.

C. Internal mobility of the immobilized layer

The values for M_2 in Table II can be compared with recent results from a study of semi-crystalline PEO studied at temperatures below the melting point.[30] At temperatures below −70 °C, the crystalline and glassy amorphous components of PEO are indistinguishable, and from fits in this temperature range $M_2(T) = [13\,500 - T \times (20\,^\circ\mathrm{C})]\ \mathrm{ms}^{-2}$ was determined. This rather weak dependence mainly subsumes thermal expansion and small-angle libration effects, and we take this value as a reference. At higher temperatures up to the melting point, the PEO helices in the crystal perform increasingly fast jumps, which in the fast limit correspond to a rigid-body rotation, reducing M_2 by a factor of about 10.

Thus, for "bulk rigid" PEO with a density similar to the amorphous or crystalline bulk phases at 70 °C, an M_2 of $12\,000\ \mathrm{ms}^{-2}$ should be expected. However, the values in Table II are almost 8 times smaller, indicating high internal mobility of the "rigid" component comparable in amplitude to what is expected and has been measured for a rotating backbone.[30]

Notably, the DQ-filtered data exhibit a Gaussian shape with in some cases even a slight modulation associated with coherent spin dynamics. This suggests that this component is in the "quasi-static" fast limit, i.e., the associated correlation time is significantly below 1 μs (slower mobility leads to intermediate-motional effects and thus β exponent values below 2). Thus, the second moment is reduced to a lower but on the time scale of FID detection constant value, with the inverse reduction factor reflecting the degree of anisotropy of the fast process. More precisely, the square root of the latter is a dynamic order parameter S,[31] which is here of the order of 0.35. This finding, along with the unexpectedly low component fractions, resolves the main source of (apparent) disagreement with earlier neutron scattering studies, which did not reveal an expected "glassy" fraction.[9,14] Although the low values for M_2 (high values of $T^*_{2,\mathrm{r}}$) were mentioned in our previous work,[13] referring to the component as "glassy" certainly caused some confusion.

D. Effect of temperature and annealing

In our previous work on poly(ethyl acrylate) (PEA) networks adsorbed on silica, a significant temperature dependence of both the immobilized fraction and the relaxation parameters was evidenced.[20] This could later be rationalized quantitatively by a gradient in effective T_g,[21] implying a gradual softening on heating. This means that what is referred to as "layer thickness" is potentially subject to definition and/or ambiguity and certainly a function of temperature. Moreover, since the long-lasting neutron scattering experiments for the PEO2k-13 series were conducted at 140 °C, the effects of high temperature and annealing are of interest.

TABLE III. Reduced-mobility fractions and relaxation parameters for sample PEO20k-42-OO at different temperatures.

Temperature (°C)	"Rigid"	Intermediate
70	$a_\mathrm{r} = 6.08\%$ $M_2 = 2620\ \mathrm{ms}^{-2}$	$a_\mathrm{i} = 7.16\%$ $T_2^* = 70.5\ \mu\mathrm{s}$ $\beta = 0.74$
110	$a_\mathrm{r} = 4.92\%$ $M_2 = 2298\ \mathrm{ms}^{-2}$	$a_\mathrm{i} = 7.65\%$ $T_2^* = 44.9\ \mu\mathrm{s}$ $\beta = 0.81$
140	$a_\mathrm{r} = 4.56\%$ $M_2 = 2189\ \mathrm{ms}^{-2}$	$a_\mathrm{i} = 7.09\%$ $T_2^* = 53.2\ \mu\mathrm{s}$ $\beta = 0.87$
After 26 h at 140		
140	$a_\mathrm{r} = 4.18\%$ $M_2 = 2189\ \mathrm{ms}^{-2}$	$a_\mathrm{i} = 6.92\%$ $T_2^* = 50.9\ \mu\mathrm{s}$ $\beta = 0.85$

The results of a temperature-variation and annealing study of the sample with the highest reduced-mobility fraction are collected in Table III. The experiments at a given temperature are typically conducted within 30 min (including temperature equilibration). At the highest temperature, the

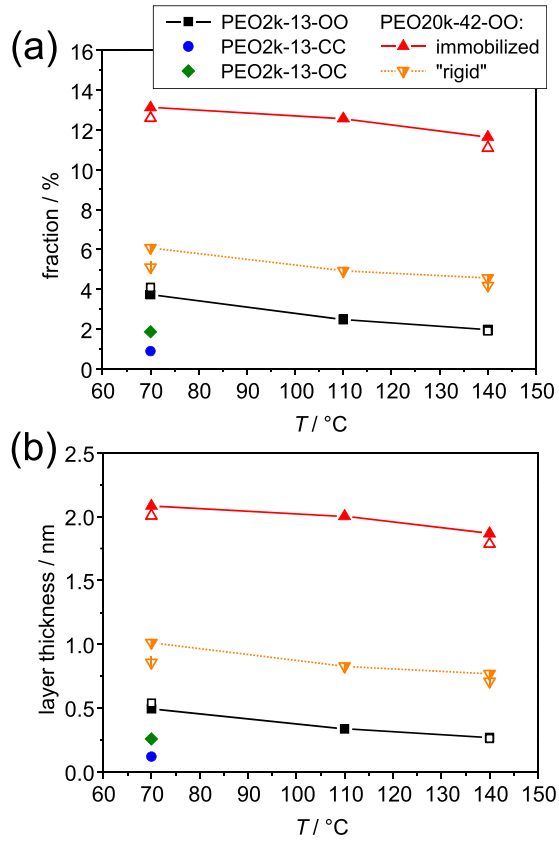

FIG. 3. (a) Total immobilized-component fractions of all samples as a function of temperature and (b) layer thickness values calculated from the same data. Open symbols are from samples measured after 26 h of annealing at 140 °C, also measured again after cooling to 70 °C. Only for sample PEO20k-42-OO the most immobilized "rigid" component is shown separately.

sample was annealed for 26 h and measured again, and yet again after cooling back to 70 °C. The results of the latter measurement are contained in Fig. 3, where all results for the component fractions and derived layer thicknesses are collected. It also contains the results of a temperature study of sample PEO2k-13-OO.

It is observed that heating causes only minor changes in the component fractions and even a counter-intuitive weak decrease in $T^*_{2,i}$ implying a stiffening. This can be explained by a speeding up of the outermost part of the layer that is then detected as mobile, and only little change in the remainder of the layer. The changes in M_2 are not much stronger than what could be expected from simple thermal expansion and enhanced small-amplitude local librations. Thus, the motional amplitude of the "backbone rotation" assumed for the most immobilized layer does not change, while the potential speeding-up of the associated correlation time is simply not detectable (as the M_2 already assumes its fast-limit value at 70 °C). Moreover, annealing at 140 °C for more than a day does not change any of the observables, and cooling back to 70 °C demonstrates full reversibility in all cases. Thus, temperature effects are rather minor, and the PEO-silica system[13] is demonstrated to behave qualitatively differently as compared to PEA-silica.[20,21]

E. Effect of water content

Since PEO is water-soluble and hygroscopic, the role of residual water contents and drying conditions should be clarified. The main effect of water concerns the most mobile component, for which it simply acts as plasticizer and speeds up the segmental dynamics. The water uptake upon exposure to RH = 100% and the loss on drying was not determined directly but was estimated from the absolute signal to be of the order of several percent. Free water is isotropically mobile and thus detected as part of the mobile polymer fraction. The effect of variations of the latter on the (relative) immobilized-component amplitudes is thus small.

The results in Table IV evidence no significant changes for the most immobilized fraction, its M_2 value, and the intermediate fraction, upon changing the water content. Only $T^*_{2,i}$ increases upon water addition and reduces to somewhat below its original value upon rigorous drying. This suggests that only a part of what is detected as intermediate fraction takes up some water behaving as plasticizer and that the usual evacuation at room temperature rather than at 50 °C leaves some small amount of water in the sample.

TABLE IV. Reduced-mobility fractions and relaxation parameters for sample PEO20k-42 upon water exposure and drying.

State	"Rigid"	Intermediate
Initial	$a_r = 5.70\%$ $M_2 = 2346\ \mathrm{ms}^{-2}$	$a_i = 7.90\%$ $T^*_2 = 68.7\ \mu\mathrm{s}$ $\beta = 0.70$
Humid	$a_r = 3.24\%$ $M_2 = 2252\ \mathrm{ms}^{-2}$	$a_i = 8.14\%$ $T^*_2 = 168.0\ \mu\mathrm{s}$ $\beta = 0.70$
Dried	$a_r = 4.65\%$ $M_2 = 2287\ \mathrm{ms}^{-2}$	$a_i = 7.72\%$ $T^*_2 = 47.7\ \mu\mathrm{s}$ $\beta = 0.82$

F. Comparison of NMR and neutron-scattering results

The fact that the NSE and TOF study of the very same PEO2k-13 samples did not provide evidence of a significant "glassy" fraction[14,15] can now be understood on the basis of the fast intra-layer mobility as evidenced by the NMR M_2 values. In addition, the neutron methods are challenged by the unexpectedly small fractions that ^{1}H NMR can still resolve. Interestingly, in a closely related earlier NSE study of PEO3k confined to cylindrical SiO_2-covered pores in silicon of about 13 nm diameter, the results were compatible with a prominent layer of about 5 nm thickness featuring either slowed-down or even negligible Rouse dynamics.[12] This may be due to the curvature effect mentioned above and stresses the complementarity of neutron-scattering and NMR results as well as the potential of joint analyses for future studies on such samples with increased immobilized fractions.

The end-group effect found for PEO2k-13 by NMR is fully in tune with the earlier NSE results. The latter data have been analyzed in terms of two dynamically distinct components, with a bulk-like fraction coexisting with an end-fixed fraction of 0.21 and 0.06 for the OO and CC samples, respectively.[14] Assuming that these fractions form a contiguous layer, Eq. (2) provides nominal thicknesses of 2.2 and 0.8 nm, respectively, which are a factor of 4 larger than what is found by NMR (see Table I). It is thus clear that most if not all of the NSE-detected end-fixed fraction must be part of what NMR detects as the mobile fraction.

In more detail, the NSE results for the end-fixed population suggested a vanishing center-of-mass diffusion and disappearing modes.[14,15] Theoretical work has discussed such an effect in terms of "mode freezing,"[32] while also the term "glassy layer" has (somewhat confusingly) been used for the same phenomenon. In the later follow-up work,[15] it was discussed that the fixation may actually arise from the formation of actual Si–O–PEO bonds upon liberation of water, which is reasonable, considering the extended measurement times at the elevated temperature of 140 °C. At the more local (segmental) scale, TOF experiments did not reveal a significant fraction of truly glassy PEO with suppressed segmental motions.[14] This is not unexpected, as only very few segments or even bonds may actually be truly "frozen" by the surface grafting. As we see now, even NMR shows no indication of truly rigid segments, suggesting high conformational flexibility of PEO monomers whose O atom provides the (physical or chemical) link to the surface.

In summary, all past and present findings can be reconciled by the fact that the immobilized layer detected by NMR represents a rather small fraction of the material that additionally features substantial internal, possibly only local rotational, mobility. While the long-time plateau of the intermediate scattering function $S(q,t)$ arising from the anisotropy of localized rotational motions would also contribute an elastic contribution to the TOF spectra, its detection was simply challenged by the dominant contribution of the SiO_2. At longer

time scales, the NSE results mainly reflect the dynamics of the NMR-mobile majority fraction. Strong lateral adsorption of multiple segments, thus a correspondingly significant immobilized layer, appears to prevail only on larger particles with low convex curvature and on flat as well as concave pore surfaces. In contrast, the lower level of lateral or end fixation prevailing on particles with diameters below the 15 nm range, in combination with high internal mobility, challenges the separate characterization of the most strongly immobilized fraction in NSE experiments.

In this way, we can thus state a high level of agreement and complementarity between the observations here and earlier neutron scattering experiments on the PEO2k samples.[14,15] Since the truncated-mode fraction found by NSE for PEO on silica[14,15] pertains to the NMR-detected mobile majority fraction, we should mention that more in-depth studies of this fraction by NMR require a more advanced (multiple-quantum) method.[33,34] For the system with larger particles and longer chains, this method has provided the quantification of a fraction of entropically active bridging chains between the particles.[13] Thus, in-depth comparisons of neutron-scattering and NMR data on the same samples will help to develop an improved understanding of confinement effects. As an example, loop-forming chains were complementarily detected recently in one and the same sample of PDMS confined to alumina pores by neutron scattering[9] and by multiple-quantum NMR.[35]

IV. SUMMARY AND CONCLUSION

Using ^{1}H NMR, we have studied the amount and properties of reduced-mobility fractions in nanocomposites made from PEO with variable endgroups and silica spheres of different sizes. It was possible to separate a most immobilized fraction and an intermediate component from the signal of the majority fraction of mobile melt-like PEO. The most immobilized fraction, although somewhat misleadingly referred to as "glassy" in previous work,[13] was found to feature fast sub-μs strongly anisotropic segmental mobility comparable to a rotation of the backbone. The intermediate fraction is characterized by only somewhat less anisotropic mobility, possibly combined with slower μs–ms larger-amplitude chain modes.

Taken together, the total immobilized fraction forms a layer of nominally 2 nm thickness on spheres of 42 nm diameter and 0.5 nm or even less on the 13 nm spheres. This curvature dependence is in tune with previous observations on other systems.[16] In the 13 nm case, a pronounced dependence on the endgroups was found, with only sub-monolayer coverage for doubly methyl-terminated chains. It was hypothesized that the larger degree of immobilization found for doubly hydroxy-terminated chains could be related to Si–O–PEO bond formation at elevated temperatures.[15] The significant end-group effect is complementary to earlier neutron-scattering results,[14,15] which suggested a partitioning of the melt-like majority fraction into an end-fixed and a free fraction. In that study, the sensitivity was not high enough to detect the small amount of reduced-mobility material related to the chain segments attached to the interface.

In the given system, the component fractions as well as the relaxation behavior (the latter dominated by the amplitude of the fast local motions) did not change appreciably upon increasing the temperature, long-time annealing, or addition of water. This behavior stands in contrast to the temperature- and solvent-activated interphase softening effects observed in other systems such as acrylate polymers[20,21] or styrene-butadiene rubber and its additives[6] adsorbed to silica. In these latter systems, the data were compatible with an apparent gradient in T_g as a function of distance from the surface and thus a broadening or apparent shift of the glass transition step in DSC experiments. Note that the crystallinity of PEO at temperatures below 60 °C interferes with such an observation in PEO-based composites.

Clearly, more systematic work is in order to clarify the origin of the observed, quite specific behavior. Variations of silica particle size, thermal treatment protocols, PEO molecular weight, and endgroups, as well as comparisons to other polymers, are clearly necessary. In this context, the advantages of ^{1}H NMR, providing robust and fast results on comparably small amounts of sample of the order of tens of mg on a high-field instrument and requiring little specific sample preparation steps, enable the necessary screening study of many samples over a wide temperature range. Such studies are currently being pursued in our laboratory.

ACKNOWLEDGMENTS

Partial funding of this work was provided by the Deutsche Forschungsgemeinschaft (DFG) Project No. SA982/4 in the framework of the priority Programme No. SPP 1369 "Polymer-Surface Contacts: Interfaces and Interphases," and Project Nos. SA982/13 and RE1025/19. We are indebted to Thomas Glomann for sample preparation and Jürgen Allgaier for the polymer synthesis of the PEO3k-13 samples, to Mansi Agarwal and Charles F. Zukoski for providing the PEO20k-42-OO sample, and to So-Youn Kim for helpful discussions.

[1] M.-J. Wang, "Effect of polymer-filler and filler-filler interactions on dynamic properties of filled vulcanizates," Rubber Chem. Technol. **71**, 520–589 (1998).
[2] A. A. Gusev, "Micromechanical mechanism of reinforcement and losses in filled rubbers," Macromolecules **39**, 5960–5962 (2006).
[3] S. Merabia, P. Sotta, and D. R. Long, "A microscopic model for the reinforcement and the nonlinear behavior of filled elastomers and thermoplastic elastomers (Payne and Mullins effects)," Macromolecules **41**, 8252–8266 (2008).
[4] J. Berriot, H. Montes, F. Lequeux, D. Long, and P. Sotta, "Evidence for the shift of the glass transition near the particles in silica-filled elastomers," Macromolecules **35**, 9756–9762 (2002).
[5] A. Papon, H. Montes, F. Lequeux, J. Oberdisse, K. Saalwächter, and L. Guy, "Solid particles in an elastomer matrix: Impact of colloid dispersion and polymer mobility modification on the mechanical properties," Soft Matter **8**, 4090–4096 (2012).
[6] A. Mujtaba, M. Keller, S. Ilisch, H.-J. Radusch, M. Beiner, T. Thurn-Albrecht, and K. Saalwächter, "Detection of surface-immobilized components and their role in viscoelastic reinforcement of rubber–silica nanocomposites," ACS Macro Lett. **3**, 481–485 (2014).
[7] N. Jiang, M. K. Endoh, T. Koga, T. Masui, H. Kishimoto, M. Nagao, S. K. Satija, and T. Taniguchi, "Nanostructures and dynamics of macromolecules bound to attractive filler surfaces," ACS Macro Lett. **4**, 838–842 (2015).
[8] J. P. Cohen-Addad, C. Roby, and M. Sauviat, "Characterization of chain binding to filler in silicone–silica systems," Polymer **26**, 1231–1233 (1985).

[9]M. Krutyeva, A. Wischnewski, M. Monkenbusch, L. Willner, J. Maiz, C. Mijangos, A. Arbe, J. Colmenero, A. Radulescu, O. Holderer, M. Ohl, and D. Richter, "Effect of nanoconfinement on polymer dynamics: Surface layers and interphases," Phys. Rev. Lett. **110**, 108303 (2013).
[10]P. Klonos, A. Kyritsis, and P. Pissis, "Interfacial and confined dynamics of PDMS adsorbed at the interfaces and in the pores of silica–gel: Effects of surface modification and thermal annealing," Polymer **84**, 38–51 (2016).
[11]M. Krutyeva, J. Martin, A. Arbe, J. Colmenero, C. Mijangos, G. J. Schneider, T. Unruh, Y. Su, and D. Richter, "Neutron scattering study of the dynamics of a polymer melt under nanoscopic confinement," J. Chem. Phys. **131**, 174901 (2009).
[12]A. Kusmin, S. Gruener, A. Henschel, N. de Souza, J. Allgaier, D. Richter, and P. Huber, "Polymer dynamics in nanochannels of porous silicon: A neutron spin echo study," Macromolecules **43**, 8162–8169 (2010).
[13]S. Y. Kim, H. W. Meyer, K. Saalwächter, and C. Zukoski, "Polymer dynamics in PEG-silica nanocomposites: Effects of polymer molecular weight, temperature and solvent dilution," Macromolecules **45**, 4225–4237 (2012).
[14]T. Glomann, G. J. Schneider, J. Allgaier, A. Radulescu, W. Lohstroh, B. Farago, and D. Richter, "Microscopic dynamics of polyethylene glycol chains interacting with silica nanoparticles," Phys. Rev. Lett. **110**, 178001 (2013).
[15]T. Glomann, A. Hamm, J. Allgaier, E. G. Hübner, A. Radulescu, B. Farago, and G. J. Schneider, "A microscopic view on the large scale chain dynamics in nanocomposites with attractive interactions," Soft Matter **9**, 10559–10571 (2013).
[16]S. E. Harton, S. K. Kumar, H. Yang, T. Koga, K. Hicks, H. Lee, J. Mijovic, M. Liu, R. S. Vallery, and D. W. Gidley, "Immobilized polymer layers on spherical nanoparticles," Macromolecules **43**, 3415–3421 (2010).
[17]N. Jouault, D. Zhao, and S. K. Kumar, "Role of casting solvent on nanoparticle dispersion in polymer nanocomposites," Macromolecules **47**, 5246–5255 (2014).
[18]J. Berriot, F. Lequeux, L. Monnerie, H. Montes, D. Long, and P. Sotta, "Filler-elastomer interaction in model filled rubbers, a ^{1}H NMR study," J. Non-Cryst. Solids **307–310**, 719–724 (2002).
[19]A. Sargsyan, A. Tonoyan, S. Davtyan, and C. Schick, "The amount of immobilized polymer in PMMA SiO_2 nanocomposites determined from calorimetric data," Eur. Polym. J. **43**, 3113–3127 (2007).
[20]A. Papon, K. Saalwächter, K. Schäler, L. Guy, F. Lequeux, and H. Montes, "Low-field NMR investigations of nanocomposites: Polymer dynamics and network effects," Macromolecules **4**, 913–922 (2011).
[21]A. Papon, K. Saalwächter, F. Lequeux, and H. Montes, "Tg gradient in nanocomposites: Evidence by NMR and DSC," Phys. Rev. Lett. **108**, 065702 (2012).
[22]N. Jouault, M. K. Crawford, C. Chi, R. J. Smalley, B. Wood, J. Jestin, Y. B. Melnichenko, L. He, W. E. Guise, and S. K. Kumar, "Polymer chain behavior in polymer nanocomposites with attractive interactions," ACS Macro Lett. **5**, 523–527 (2016).
[23]C. Rotella, M. Wübbenhorst, and S. Napolitano, "Probing interfacial mobility profiles via the impact of nanoscopic confinement on the strength of the dynamic glass transition," Soft Matter **7**, 5260–5266 (2011).
[24]M. Füllbrandt, P. J. Purohit, and A. Schönhals, "Combined FTIR and dielectric investigation of poly(vinyl acetate) adsorbed on silica particles," Macromolecules **46**, 4626–4632 (2013).
[25]W.-K. Rhim, A. Pines, and J. S. Waugh, "Time-reversal experiments in dipolar-coupled spin systems," Phys. Rev. B **3**, 684–696 (1971).
[26]S. Matsui, "Solid-state NMR imaging by magic sandwich echoes," Chem. Phys. Lett. **179**, 187–190 (1991).
[27]D. E. Demco, A. Johansson, and J. Tegenfeldt, "Proton spin diffusion for spatial heterogeneity and morphology investigations of polymers," Solid State Nucl. Magn. Reson. **4**, 13–38 (1995).
[28]M. Mauri, Y. Thomann, H. Schneider, and K. Saalwächter, "Spin diffusion NMR at low field for the study of multiphase solids," Solid State Nucl. Magn. Reson. **34**, 125–141 (2008).
[29]K. Schäler, M. Roos, P. Micke, Y. Golitsyn, A. Seidlitz, T. Thurn-Albrecht, H. Schneider, G. Hempel, and K. Saalwächter, "Basic principles of static proton low-resolution spin diffusion NMR in nanophase-separated materials with mobility contrast," Solid State Nucl. Magn. Reson. **72**, 50–63 (2015).
[30]R. Kurz, A. Achilles, W. Chen, M. Schäfer, A. Seidlitz, Y. Golitsyn, J. Kressler, T. Miyoshi, T. Thurn-Albrecht, and K. Saalwächter, "Intracrystalline jump motion in poly(ethylene oxide) lamellae of variable thickness–a comparison of NMR methods," Macromolecules (submitted).
[31]D. Reichert and K. Saalwächter, "Dipolar coupling: Molecular-level mobility," in *NMR Crystallography*, edited by R. K. Harris, R. E. Wasylishen, and M. J. Duer (John Wiley and Sons, Chichester, 2009), pp. 177–193.
[32]T. A. Vilgis, G. Heinrich, and M. Klüppel, *Reinforcement of Polymer Nano-Composites* (Cambridge University Press, Cambridge, 2009).
[33]F. Vaca Chávez and K. Saalwächter, "NMR observation of entangled polymer dynamics: Tube model predictions and constraint release," Phys. Rev. Lett. **104**, 198305 (2010).
[34]S. Ok, M. Steinhart, A. Şerbescu, C. Franz, F. Vaca Chávez, and K. Saalwächter, "Confinement effects on chain dynamics and local chain order in entangled polymer melts," Macromolecules **43**, 4429–4434 (2010).
[35]C. Franz, F. Lange, Y. Golitsyn, B. Hartmann-Azanza, M. Steinhart, M. Krutyeva, and K. Saalwächter, "Chain dynamics and segmental orientation in polymer melts confined to nanochannels," Macromolecules **49**, 244–256 (2016).